First-Principles Study of Titania Nanoribbons: Formation, Energetics, and Electronic Properties

ARTICLE *in* THE JOURNAL OF PHYSICAL CHEMISTRY C · MAY 2010

Impact Factor: 4.77 · DOI: 10.1021/jp912143p

First-Principles Study of Titania Nanoribbons: Formation, Energetics, and Electronic Properties

Tao He, Fengchun Pan, Zexiao Xi, Xuejuan Zhang, Hongyu Zhang, Zhenhai Wang, Mingwen Zhao,* Shishen Yan, and Yueyuan Xia

School of Physics and State Key Laboratory of Crystal Materials, Shandong University, Jinan 250100, Shandong, China

Received: December 24, 2009; Revised Manuscript Received: April 9, 2010

The geometric, electronic, and magnetic properties of titania nanoribbons (TiO_2NRs) are investigated with use of first-principles calculations within density-functional theory. The TiO_2NRs formed by cutting ultrathin TiO_2 nanosheet along armchair and zigzag axes have high energetic stability. Zigzag TiO_2NRs are more preferable than armchair ones. The electronic structures of TiO_2NRs highly depend on the growth orientation and the ribbon width. Introducing oxygen vacancy defects into the edges of zigzag TiO_2NRs under poor oxygen conditions can reduce the band gap and trigger the spin-polarization of edge states. These TiO_2NRs with well-defined atomic structures, high stability, and tunable electronic properties are expected to have potential applications in solar cells, spintronic devices, and sensors.

Introduction

One-dimensional (1D) nanomaterials, such as nanowires, nanotubes, and nanoribbons, have been the subject of intensive research during the past two decades, because of the fundamental scientific interest in nanoscale-confined systems as well as the intriguing properties that are expected to be important for future nanodevices.[1] Recently, graphene nanoribbons (GNRs), which are geometrically terminated single graphite layers, have gained considerable attention.[2−11] In contrast to single-walled carbon nanotubes (CNTs), GNRs possess nonzero band gaps regardless of the edge shapes.[3] More interestingly, the edge states of the zigzag-edged GNRs are spin-polarized due to symmetry-breakage, favoring a ground state with an opposite spin orientation across the ribbon between ferromagnetically ordered edge states on each zigzag edge.[2,7,8] By applying transverse electric field to zigzag GNRs, half-metallicity can be achieved, rending them promising candidate materials for spintronic devices.[2,7,8] The electronic and magnetic properties of GNRs can also be modulated by doped impurities,[12,13] or adsorbed molecules.[14−18] In addition, experimental realization of GNRs with various widths and crystallographic orientations is more facilitative and flexible than CNTs, through standard lithographic procedures or chemical methords.[5,6,9]

Inspired by the unique properties of GNRs, much effort has been paid in finding nanoribbons of other materials, such as boron nitride (BNNRs),[19−22] molybdenum disulfide (MoS_2NRs),[23] silicon carbide (SiCNRs),[24] and zinc oxide (ZnONRs).[25,26] The single-layered materials of these materials are semiconducting with wide band gaps, in contrast to zero-band gap graphene. However, spin-polarization of the edge states has been predicted for these nanoribbons, which is sensitive to edge termination. Recently, metallic boron nanoribbons (BNRs) have also been predicted.[27] These works extend the applications of inorganic nanoribbons in nanoscaled devices.

Titanium oxide (TiO_2) is a versatile oxide semiconductor for its fascinating performance in fields ranging from photocatalyst,[28−30] chemical gas sensor,[31] self-cleaning and antiseptic coatings,[30] dye-sensitized solar cells (DSSCs),[32,33] to spintronic devices.[34] Considerable theoretical works have been devoted to the geometric and electronic properties of zero-dimensional (0D),[35−40] one-dimensional (1D),[41−44] and two-dimensional (2D)[41,44,45] TiO_2 nanomaterials using first-principles calculations or tight-binding methods. Experimentally, an ultrathin TiO_2 nanosheet ($UTiO_2$NS) consisting of an O−Ti−O trilayer has been synthesized by evaporating Ti atoms on oxygen chemisorbed Cu(100) or Fe/Cu(100) substrate,[46] or by evaporating Ti atoms in O_2 ambience on Ru(0001) substrate and subsequent annealing process.[47] The ultrastability of isolated $UTiO_2$NS has been confirmed in some previous works, which is attributed to the structural feature that each atom is fully coordinated.[48,49] Due to the quantum-confinement effect, $UTiO_2$NS has a band gap wider than that of bulk crystal.[48,49] A pronounced blue shift of the excitonic transition peak[50] and rapid electron transport over bulk[47,51] have been revealed for this two-dimensional material. However, the large band gap hinders the applications of $UTiO_2$NS in solar cell devices, although it has a higher surface-to-bulk ratio compared to that of bulk crystal. Therefore, modifying the electronic properties of $UTiO_2$NS is quite necessary.

It is rationally expected that the TiO_2 nanoribbons (TiO_2NRs) can be produced from $UTiO_2$NS, probably via the well-established technique of fabricating GNRs from graphene. The orientation, edge structure, and ribbon width of TiO_2NRs provides abundant freedoms to tune their electronic properties. Here, we report our first-principles study on the stable configurations, electronic structures, and magnetic properties of TiO_2NRs. We found that both armchair and zigzag TiO_2NRs prefer stable oxygen-terminated edge structures. Perfect TiO_2NRs are spin-unpolarized wide-band gap semiconductors with variable band gap values depending on their growth orientation and width. Oxygen vacancy (V_O) defects can be easily formed in the region near the edges of TiO_2NRs, which trigger spin-polarization of edge states in a ferromagnetic way. The V_O-containing TiO_2NRs exhibit the features of narrow-band gap semiconductors or half-metals depending on the V_O

* To whom correspondence should be addressed. E-mail: zmw@sdu.edu.cn.

10.1021/jp912143p
Published on Web 05/03/2010

concentrations. Our work offers a promising route toward fabricating low-dimensional TiO_2 nanomaterials which have potential applications in solar cells and spintronic devices.

Methods and Computational Details

Our calculations are on the basis of density-functional theory (DFT) in conjunction with a projector-augmented wave (PAW) method,[52,53] which is implemented in the Vienna ab initio simulation package (VASP).[54] Generalized gradient approximation (GGA) in the form of PW91 is employed for the exchange-correlation functional.[55] Both atomic positions and lattice constants are fully relaxed with use of the conjugate gradient (CG) procedure without any symmetric constraints. Atomic forces are converged to 0.01 eV/Å, and the precision for the total energy calculations is 0.1 meV. The energy cutoffs used for plane-wave expansion of electron wave functions are 450 eV for all elements. The Brillouin zone is sampled on a grid of $8 \times 1 \times 1$ k points for the TiO_2NRs growing along the x direction. Vacuum spaces up to 30 Å are applied to exclude the interactions between images. We also consider on-site Coulomb repulsion U of the Ti 3d orbital using a local spin density approximation (L(S)DA+U) to overcome the deficiency of GGA functional in the calculations of band gap structures and magnetic ground states. The effective $U = 5.8$ eV of the Ti 3d orbital used in this work gives the band gap values of both rutile and anatase TiO_2 comparable to the experimental data.[49]

Results and Discussion

The model structures of TiO_2NRs were generated by cutting an UTiO_2NS along armchair and zigzag orientations, which are referred to as zigzag TiO_2NRs (ZTiO_2NRs) and armchair TiO_2NRs (ATiO_2NRs), as shown in Figure 1a,b. The TiO_2NRs with different widths are classified by the number of Ti lines (N_Z or N_A) across the ribbon width as shown in Figure 1, and are denoted as N_Z-ZTiO_2NRs and N_A-ATiO_2NRs, respectively. For ZTiO_2NRs, there are two kinds of edge structures, one is O-terminated, another is Ti-terminated, as shown in Figure 1a,c. A series of N_Z-ZTiO_2NRs ($2 \le N_Z \le 10$) and N_A-ATiO_2NRs ($3 \le N_A \le 18$) up to width of 2.5 nm are calculated. Slight distortion occurs near the edges of ATiO_2NRs and O-terminated ZTiO_2NRs, both of which are stoichiometric. For example, the nearest Ti−O distance at the edges of 6-ZTiO_2NR and 10-ATiO_2NR shortens to 1.86 Å, compared to that of 1.99 Å in UTiO_2NS,[49] whereas the averaged Ti−O bond lengths (2.02 and 1.95 Å) in the central region of these nanoribbons are close to that of UTiO_2NS. Particularly, the O atoms at the edge of ATiO_2NRs move outward by 0.32 Å relative to the edge Ti atoms. Therefore, ATiO_2NRs are terminated by O atoms rather than Ti−O dimers. We also considered the Ti-terminated ZTiO_2NRs which are nonstoichiometric, as shown in the left panel of Figure 1c. The O atoms next to the edge Ti atoms move to the edge after geometric optimization, forming an O-terminated configuration accompanied by formation of O vacancies near the edge, as shown in the right panel of Figure 1c. The Ti−O bond length at the edge is 1.86 Å. Such edge reconstruction is related to the Coulomb repulsion between O anions near the edge. Therefore, O-termination is an intrinsic characteristic for all the TiO_2NRs.

Considering that the UTiO_2NS has been synthesized,[46,47] the relative energy (E_R) of TiO_2NRs per TiO_2 unit with respect to UTiO_2NS can be used to evaluate their stability and plausibility. The E_R evolution of TiO_2NRs as a function of ribbon width is plotted in Figure 2a. It is obvious that the E_R values for both

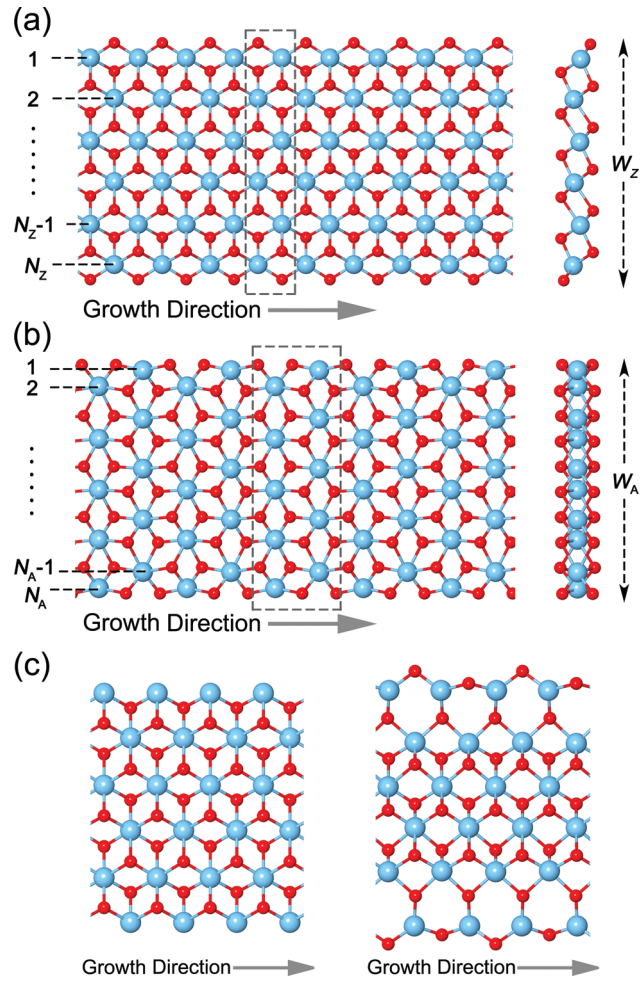

Figure 1. Top and side views of (a) ZTiO_2NR and (b) ATiO_2NR, and (c) the unrelaxed Ti-terminated ZTiO_2NR (left) relaxed to an O-terminated ZTiO_2NR (right). The big cyan balls are Ti atoms and the small red balls are O atoms. Gray dashed frameworks denote the unitcells. The variable N_Z and N_A represent the numbers of Ti rows aligned perpendicularly to the ZTiO_2NR and ATiO_2NR growth direction, respectively. W_Z and W_A are the width of ZTiO_2NR and ATiO_2NR, respectively.

ATiO_2NRs and ZTiO_2NRs decrease with the increase of ribbon width (W) and can be fitted using the expression $E_R = c/W$, with the fitting parameter of $c = 2.69$ eV·Å/TiO_2 for ZTiO_2NRs and $c = 4.06$ eV·Å/TiO_2 for ATiO_2NRs. The energy increase of TiO_2NRs with respect to UTiO_2NS arises from the TiO_2 units at the edges which contain under-coordinated O and Ti atoms and undergo structural distortion, because the structural distortion occurs mainly at the edges. The relative energy of TiO_2NRs can be written as $E_R = 2\Delta/N$, where Δ is the energy increase per edge TiO_2 unit, and $N = N_Z$ or N_A, which is proportional to W. The linear relationship between E_R and the inverse of W can be obtained, provided that the energy increase per edge TiO_2 unit (Δ) is constant. The fitting data of Δ are 0.49 eV/TiO_2 and 1.42 eV/TiO_2 for ZTiO_2NRs and ATiO_2NRs, respectively.

The plausibility of TiO_2NRs can also be hinted by their cleavage energy (E_C) which corresponds to the energy cost to generate a TiO_2NR by cutting an UTiO_2NS. The E_C values of TiO_2NRs are calculated using the expression $E_C = 2 \times (E_{NR} - n \times E_0)/L$, where E_{NR} is the total energy per supercell of TiO_2NR, n is the number of TiO_2 units per supercell, E_0 is the total energy per TiO_2 unit of UTiO_2NS, and L is the supercell length of TiO_2NR. The variation of E_C as a function of TiO_2NR width is shown in Figure 2b. The E_C values oscillate between

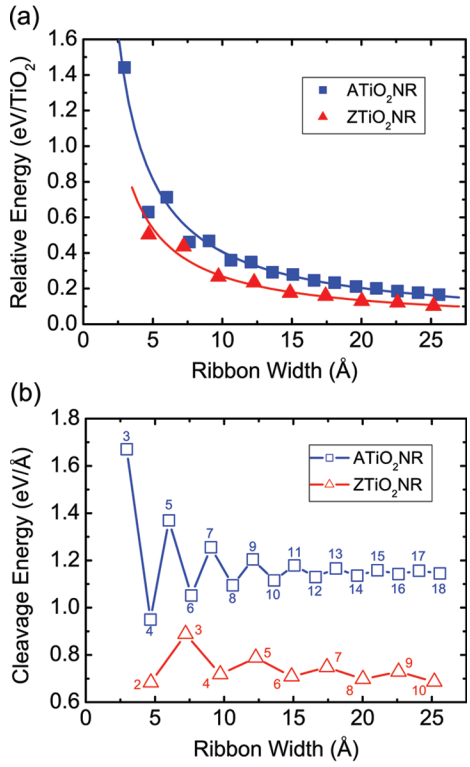

Figure 2. (a) Relative energy (E_R) and (b) cleavage energy (E_C) evolutions of $ZTiO_2$NRs and $ATiO_2$NRs as a function of ribbon width. The relative energy is fitted by the formula $E_R = c/W$. The N_Z and N_A values are represented by red and blue numbers, respectively.

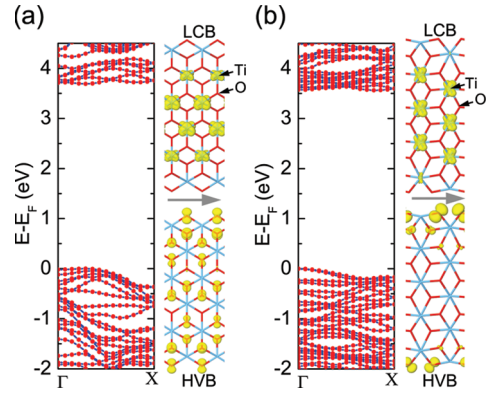

Figure 3. Band structures (left) and band-decomposed electron density isosurfaces (right) of LCB and HVB at the Γ point for (a) 6-$ZTiO_2$NR and (b) 10-$ATiO_2$NR. The isovalue is 0.01 |e|/Å^3. The arrow indicates the growth direction of the ribbons.

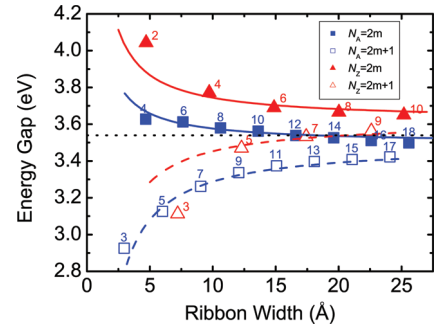

Figure 4. Energy gap evolution of $ZTiO_2$NRs (triangles) and $ATiO_2$NRs (squares) as a function of ribbon width. The solid symbols represent the ribbons with $N = 2$ m while the hollow symbols represent the ribbons with $N = 2m + 1$, where $N = N_Z$ or N_A and m is a positive integer. The band gaps are fitted by the formula $E_g = a + b/W$, where the fitting parameters a and b are 3.49 and 0.82 eV·Å for $ATiO_2$NRs with even N_A; 3.49 and −2.07 eV·Å for $ATiO_2$NRs with odd N_A; 3.62 and 1.23 eV·Å for $ZTiO_2$NRs with even N_Z; and 3.62 and −1.68 eV·Å for $ZTiO_2$NRs with odd N_Z. The dotted line indicates the band gap value of $UTiO_2$NS in ref 49.

even and odd N_Z (or N_A) and converge to the values of 0.65 eV/Å for $ZTiO_2$NRs and 1.1 eV/Å for $ATiO_2$NRs, respectively, as they are wide enough. The oscillation of E_C values for narrow TiO_2NRs is due to the attractive (even) and repulsive (odd) interactions between the two edges. When a TiO_2NR contains an even number of Ti lines, the 2-fold-coordinated O atoms at one edge interact attractively with the under-coordinated Ti atoms at the opposite edge, whereas for the TiO_2NR containing an odd number of Ti lines, the O atoms at two edges interact repulsively. This is the reason why E_R values of TiO_2NRs with small widths deviate from the fitting curves shown in Figure 2a. The lower E_C values of $ZTiO_2$NRs than $ATiO_2$NRs imply that the formation of $ZTiO_2$NRs by cutting an $UTiO_2$NS is energetically preferable. This is related to the low density of under-coordinated Ti and O atoms at the edge of $ZTiO_2$NRs.

The electronic structures of TiO_2NRs were then studied by using the L(S)DA+U scheme. All the stoichiometric TiO_2NRs are semiconductors with band gaps ranging from 2.93 to 4.04 eV. $ZTiO_2$NRs have indirect band gaps, whereas $ATiO_2$NRs possess direct band gaps at the Γ point, as shown in Figure 3a,b. The band-resolved electron density of the lowest conduction band (LCB) and the highest valence band (HVB) shows that the 3d states of the "bulk" Ti atoms contribute to the LCB of $ZTiO_2$NRs and $ATiO_2$NRs. The HVB of $ZTiO_2$NRs arises from the 2p states of all the O atoms, whereas for $ATiO_2$NRs, it originates from the 2p states of the edge O atoms which are 2-fold-coordinated.

Figure 4 gives the band gaps (E_g) of $ZTiO_2$NRs and $ATiO_2$NRs versus their widths obtained with the L(S)DA+U scheme. It is interesting to see that the band gaps as a function of ribbon width are separated into two different categories for both armchair and zigzag nanoribbons with a hierarchy of gap size given by $E_{g,2m} > E_{g,2m+1}$, as shown in Figure 4. For the nanoribbons with N_Z (or N_A) = $2m$ (where m is a positive integer), the E_g values decrease with the increase of ribbon width, whereas for those with $N_Z = 2m + 1$ (or $N_A = 2m + 1$), the E_g values increase with the increase of ribbon width. The band gaps of $ZTiO_2$NRs and $ATiO_2$NRs do not converge to the same value even when the ribbons are very wide. For $ZTiO_2$NRs, the fitting band gap of infinite width is 0.08 eV larger than that of $UTiO_2$NS, while for $ATiO_2$NRs, it is 0.05 eV smaller than that of $UTiO_2$NS. The DFT Kohn−Sham eigenvalues within LDA generally underestimate the band gap of materials. By taking the on-site Coulomb repulsion of Ti 3d orbitals into account, the LDA band gap of rutile-TiO_2 is corrected to 2.43 eV, still 0.57 eV smaller than the experimental value.[49] The accurate first-principles calculation of band gaps requires a quasiparticle approach. However, the basic physics discovered here should not be changed.

It is interesting to compare the band gap evolution of TiO_2NRs with those of other nanoribbons, such as GNRs,[3] BNNRs,[19] and SiCNRs,[24] which possess similar honeycomb atomic arrangements. The band gaps of armchair GNRs, BNNRs, and SiCNRs as a function of ribbon widths are separated into three categories, whereas those of zigzag GNRs and BNNRs decrease monotonously with increasing ribbon width. The three-family behavior of armchair GNR band gaps has been explained by using a tight-binding (TB) model for

the π electrons,[3] and seems to be a common feature of armchair nanoribbons with honeycomb atomic arrangements, although the variational trends differ for different materials.[3,19,24] By contrast, both armchair and zigzag TiO_2NRs exhibit two-family band gap evolution. The physical origin of this two-family behavior differs from that of the three-family feature of GNRs, since the TiO_2NRs have much more complicated atomic arrangements than GNRs and there are no π electrons in TiO_2NRs. It is noteworthy that the cleavage energies versus ribbon widths also exhibit a two-family behavior, as shown in Figure 2b, suggesting that band gap evolution may be related to the interactions between two edges. We deduce that the Coulomb repulsive (attractive) interactions between the two edges of TiO_2NRs containing an odd (even) number of Ti lines increase (decrease) the HVB of nanoribbons, making the band gaps oscillate between odd and even N_Z (or N_A).

Unlike zigzag-edge GNRs, the edge states of TiO_2NRs are spin-unpolarized. This is because the Ti atoms in the stoichiometric TiO_2NRs are at +4 charge states and the 3d orbitals are empty. No unpaired electron appears at the edges. However, this condition can be changed by introducing oxygen vacancies into TiO_2NRs to form nonstoichiometric TiO_{2-x}NRs. Under poor oxygen conditions, the formation energy (ΔE) of an oxygen vacancy can be evaluated by using the expression $\Delta E = (E_{V_O} - E_0 + n\mu_O)/n$, where E_{V_O} and E_0 are the total energies of defective and perfect TiO_2NRs, respectively, and n is the number of oxygen vacancies. The chemical potential of oxygen atom, μ_O, equals $(\mu_{TiO_2} - \mu_{Ti})/2$, where μ_{TiO_2} is the chemical potential of a TiO_2 unit in rutile and μ_{Ti} is the chemical potential of the Ti atom calculated from the Ti crystal. Our calculations show that oxygen vacancy defects prefer to form at the sites close to the outmost oxygen atoms of ZTiO_2NRs with negative values of ΔE, e.g., −0.6 eV per V_O for 6-ZTiO_2NR, whereas the ΔE values of other sites are positive. First, we considered a nonstoichiometric TiO_{2-x}NR formed by introducing one V_O line along one edge of ZTiO_2NR, whose structure can be regarded as the relaxed configuration of one-side Ti-terminated ZTiO_2NRs. The edge Ti atoms are 3-fold-coordinated with one unpaired 3d electron per Ti atom. Unsurprisingly, these Ti 3d electrons interact ferromagnetically mediated by the 2p states of the edge oxygen atoms, as shown in Figure 5a, following the superexchanging mechanism. The band gap (Figure 5b) of the spin-up branch is only 0.06 eV, while that of the spin-down branch is as large as 2.31 eV.

We then considered the 6-ZTiO_2NR with V_O defects formed at both edges, as shown in Figure 5c. The net spin-up electron density ($\rho_\uparrow$) of Ti 3d mainly locates in the central region while the net spin-down electron density ($\rho_\downarrow$) is confined at the edges, giving rise to ferromagnetic ordering between two edges. More interestingly, the spin-up branch shows metallicity with two degenerate bands across the Fermi level, while the spin-down branch has a band gap of 2.39 eV, exhibiting the feature of half-metal, as shown in Figure 5d. We also calculated the spin configuration, which has the spins of the two edges ordered in an antiferromagnetic way, and found that it is energetically less stable than that of ferromagnetic ordering by about 137.66 meV/cell. Moreover, the spin-polarization energy calculated by the energy difference between the spin-unpolarized phase and the spin-polarized phase is 2961.61 meV/cell. These results imply that the half-metallicity in ZTiO_{2-x}NR is robust even at room temperature.

The spin-polarization in ZTiO_{2-x}NRs is eliminated when two H atoms are incorporated into one V_O, as shown in Figure 5e. The H atoms prefer to locate either on the V_O site or above the edge Ti atoms. The average Ti−H distance is 1.96 Å. The impurity bands are removed from the band gap and the magnetic moments are quenched due to the passivation of unpaired Ti 3d electrons. However, the formation energy of hydrogenation is calculated to be only −0.25 eV/H, suggesting that the H atoms can be easily desorbed.

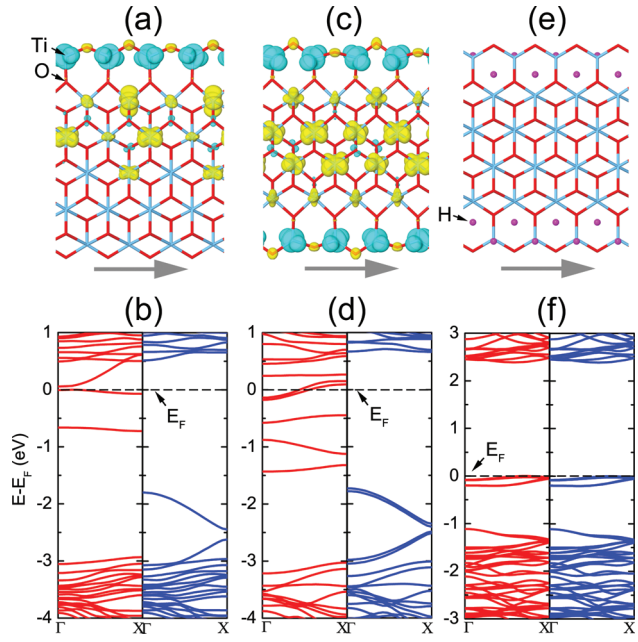

Figure 5. The isosurfaces of spin density $\rho = \rho_\uparrow - \rho_\downarrow$ (top) and the band structures (bottom) of 6-ZTiO_{2-x}NRs with V_O-defected one edge (left), two edges (middle), and hydrogenated V_O defects at two edges (right). The isovalue is 0.01 |e|/Å^3. Yellow and cyan surfaces represent the spin-up and spin-down, respectively. Band lines of spin-up and spin-down branches are represented by red and blue lines. The energy at the Fermi level (E_F) is set to zero.

It is noteworthy that the TiO_2NRs synthesized in recent experiments[56−58] have large size (>100 nm in width) and rutile or anatase structures, which are quite different from the ultrathin TiO_2NRs present in this work. The metastability of the ultrathin TiO_2NRs compared to rutile or anatase configuration implies the difficulty for experimental realization. However, the already-synthesized UTiO_2NS[46,47] hints at the plausibility of these ultrathin TiO_2NRs, analogous to the generation of GNRs from graphene.

Conclusions

Our first-principles calculations indicate that TiO_2NRs can be formed from the already-synthesized UTiO_2NS. Zigzag TiO_2NRs terminated by oxygen atoms are energetically more preferable than the armchair ones with the same ribbon width. Both zigzag and armchair TiO_2NRs are semiconductors with a band gap larger than 2.93 eV, in our L(S)DA+U procedure. The band gaps as a function of ribbon width are separated into two different categories with a hierarchy of gap size given by $E_{g,2m} > E_{g,2m+1}$. For the TiO_2NRs containing an even number of Ti lines (N_Z or $N_A = 2m$), the band gap ($E_{g,2m}$) decreases with the increase of width, whereas for the TiO_2NRs with N_Z (or N_A) $= 2m + 1$, the band gap ($E_{g,2m+1}$) increases with increasing width. The spin-polarization of edge states can be achieved in the nonstoichiometric TiO_2NRs containing 3-fold-coordinated Ti atoms at the edge, which may be formed under poor oxygen conditions. When V_O defects are formed at one edge of TiO_2NRs, the spin-up branch has a band gap of 0.06 eV, while the band gap of the spin-down branch is 2.31 eV. When V_O

defects are formed at both edges, the TiO_{2-x}NR becomes a half-metal. The hydrogenation of V_O defects quenches the magnetic moments. The tunable band gaps, half-metallicity, and the sensitivity to H atoms of ultrathin TiO_2NRs containing V_O defects imply their potential applications in solar cells, spintronics-based devices, and sensors.

Acknowledgment. This work described in this paper is supported by the National Natural Science Foundation of China (Grant No. 10974119), the National Basic Research 973 Program of China (Grant No. 2005CB623602), and the Independent Innovation Foundation of Shandong University (IIFSDU, Grant No. 2009JQ003).

References and Notes

(1) Xia, Y.; Yang, P.; Sun, Y.; Wu, Y.; Mayers, B.; Gates, B.; Yin, Y.; Kim, F.; Yan, H. *Adv. Mater.* **2003**, *15*, 353.
(2) Son, Y.; Cohen, M. L.; Louie, S. G. *Nature* **2006**, *444*, 347.
(3) Son, Y.; Cohen, M. L.; Louie, S. G. *Phys. Rev. Lett.* **2006**, *97*, 216803.
(4) Ezawa, M. *Phys. Rev. B* **2006**, *73*, 045432.
(5) Han, M. Y.; Özyilmaz, B.; Zhang, Y.; Kim, P. *Phys. Rev. Lett.* **2007**, *98*, 206805.
(6) Li, X.; Wang, X.; Zhang, L.; Lee, S.; Dai, H. *Science* **2008**, *319*, 1229.
(7) Kan, E.-J.; Li, Z.; Yang, J.; Hou, J. G. *Appl. Phys. Lett.* **2007**, *91*, 243116.
(8) Hod, O.; Barone, V.; Peralta, J. E.; Scuseria, G. E. *Nano Lett.* **2007**, *7*, 2295.
(9) Yan, Q. M.; Huang, B.; Yu, J.; Zheng, F. W.; Zang, J.; Wu, J.; Gu, B. L.; Liu, F.; Duan, W. H. *Nano Lett.* **2007**, *7*, 1469.
(10) Koskinen, P.; Malola, S.; Häkkinen, H. *Phys. Rev. Lett.* **2008**, *101*, 115502.
(11) Lakshmi, S.; Roche, S.; Cuniberti, G. *Phys. Rev. B* **2009**, *80*, 193404.
(12) Dutta, S.; Manna, A. K.; Pati, S. K. *Phys. Rev. Lett.* **2009**, *102*, 096601.
(13) Li, Y.; Zhou, Z.; Shen, P.; Chen, Z. *ACS Nano* **2009**, *3*, 1952.
(14) Kan, E.-J.; Li, Z.; Yang, J.; Hou, J. G. *J. Am. Chem. Soc.* **2008**, *130*, 4224.
(15) Li, Y.; Zhou, Z.; Shen, P.; Chen, Z. *J. Phys. Chem. C* **2009**, *113*, 15043.
(16) Wassmann, T.; Seitsonen, A. P.; Saitta, A. M.; Lazzeri, M.; Mauri, F. *Phys. Rev. Lett.* **2008**, *101*, 096402.
(17) López-Bezanilla, A.; Triozon, F.; Roche, S. *Nano Lett.* **2009**, *9*, 2537.
(18) Cantele, G.; Lee, Y.-S.; Ninno, D.; Marzari, N. *Nano Lett.* **2009**, *9*, 3425.
(19) Park, C.-H.; Louie, S. G. *Nano Lett.* **2008**, *8*, 2200.
(20) Ding, Y.; Wang, Y.; Ni, J. *Appl. Phys. Lett.* **2009**, *94*, 233107.
(21) Chen, W.; Li, Y.; Yu, G.; Zhou, Z.; Chen, Z. *J. Chem. Theory Comput.* **2009**, *5*, 3088.
(22) Chen, W.; Li, Y.; Yu, G.; Li, C.-Z.; Zhang, S. B.; Zhou, Z.; Chen, Z. *J. Am. Chem. Soc.* **2010**, *132*, 1699.
(23) Li, Y.; Zhou, Z.; Zhang, S.; Chen, Z. *J. Am. Chem. Soc.* **2008**, *130*, 16739.
(24) Sun, L.; Li, Y.; Li, Z.; Li, Q.; Zhou, Z.; Chen, Z.; Yang, J.; Hou, J. G. *J. Chem. Phys.* **2008**, *129*, 174114.
(25) Yan, H.; Johnson, J.; Law, M.; He, R.; Knutsen, K.; Mckinney, J. R.; Pham, J.; Saykally, R.; Yang, P. *Adv. Mater.* **2003**, *15*, 1907.
(26) Botello-Méndez, A. R.; López-Urías, F.; Terrones, M.; Terrones, H. *Nano Lett.* **2008**, *8*, 1562.
(27) Ding, Y.; Yang, X.; Ni, J. *Appl. Phys. Lett.* **2008**, *93*, 043107.
(28) Fujishima, A.; Honda, K. *Nature* **1972**, *238*, 37.
(29) Anpo, M.; Takeuchi, M. *J. Catal.* **2003**, *216*, 505.
(30) Fujishima, A.; Hashimoto, K.; Watanabe, T. *TiO_2 Photocatalysis. Fundamentals and Applications*; BKC, Inc.: Tokyo, Japan, 1999; pp 14−176.
(31) Akbar, S.; Yoo, S. *Chem. Senses* **2004**, *20*, 30.
(32) Mor, G. K.; Shanka, K.; Paulose, M.; Varghese, O. K.; Grimes, C. A. *Nano Lett.* **2006**, *6*, 215.
(33) Tan, B.; Wu, Y. *J. Phys. Chem. B* **2006**, *110*, 15932.
(34) Gao, G. Y.; Yao, K. L.; Liu, Z. L.; Zhang, J.; Li, X. L.; Zhang, J. Q.; Liu, N. *J. Magn. Magn. Mater.* **2007**, *313*, 210.
(35) Persson, P.; Bergström, R.; Lunell, S. *J. Phys. Chem. B* **2000**, *104*, 10348.
(36) Lundqvist, M. J.; Nilsing, M.; Persson, P.; Lunell, S. *Int. J. Quantum Chem.* **2006**, *106*, 3214.
(37) Barnard, A. S.; Erdin, S.; Lin, Y.; Zapol, P.; Halley, J. W. *Phys. Rev. B* **2006**, *73*, 205405.
(38) Koparde, V. N.; Cumming, P. T. *J. Phys. Chem. C* **2007**, *111*, 6920.
(39) Erdin, S.; Lin, Y.; Halley, J. W.; Zapol, P.; Redfern, P.; Curtiss, L. *J. Electroanal. Chem.* **2007**, *607*, 147.
(40) Iacomino, A.; Cantele, G.; Ninno, D.; Marri, I.; Ossicini, S. *Phys. Rev. B* **2008**, *78*, 075405.
(41) Enyashin, A. N.; Seifert, G. *Phys. Status Solidi B* **2005**, *242*, 1361.
(42) Meng, S.; Ren, J.; Kaxiras, E. *Nano Lett.* **2008**, *8*, 3266.
(43) Zhang, D.; Liu, P.; Liu, C. *J. Phys. Chem. C* **2008**, *112*, 16729.
(44) Casarin, M.; Vittadini, A.; Selloni, A. *ACS Nano* **2009**, *3*, 317.
(45) Alvarez-Ramirez, F.; Ruiz-Morales, Y. *Chem. Mater.* **2007**, *19*, 2947.
(46) Maeda, T.; Kobayashi, Y.; Kishi, K. *Surf. Sci.* **1999**, *436*, 249.
(47) Männig, A.; Zhao, Z.; Rosenthal, D.; Christmann, K.; Hoster, H.; Rauscher, H.; Behm, R. J. *Surf. Sci.* **2005**, *576*, 29.
(48) Wang, J. G.; Wang, L.; Ma, L.; Zhao, J. J.; Wang, B. L.; Wang, G. H. *Phys. E* **2009**, *41*, 838.
(49) He, T.; Zhao, M. W.; Zhang, X. J.; Zhang, H. Y.; Wang, Z. H.; Xi, Z. X.; Liu, X. D.; Yan, S. S.; Xia, Y. Y.; Mei, L. M. *J. Phys. Chem. C* **2009**, *113*, 13610.
(50) Sasaki, T.; Watanabe, M. *J. Phys. Chem. B* **1997**, *101*, 10159.
(51) Freund, H. J. *Surf. Sci.* **2002**, *500*, 271.
(52) Blöchl, P. E. *Phys. Rev. B* **1994**, *50*, 17953.
(53) Kresse, G.; Joubert, J. *Phys. Rev. B* **1999**, *59*, 1758.
(54) Kresse, G.; Furthmüller, J. *Phys. Rev. B* **1996**, *54*, 11169. Kresse, G.; Furthmüller, J. *Comput. Mater. Sci.* **1996**, *6*, 15.
(55) Perdew, J. P.; Wang, Y. *Phys. Rev. B* **1992**, *45*, 13244.
(56) Amin, S. S.; Nicholls, A. W.; Xu, T. T. *Nanotechnology* **2007**, *18*, 445609.
(57) Yu, Q.; Wang, M.; Chen, H. *Mater. Lett.* **2010**, *64*, 428.
(58) Li, Q.; Liu, B.; Wang, L.; Li, D.; Liu, R.; Zou, B.; Cui, T.; Zou, G.; Meng, Y.; Mao, H.-K.; Liu, Z.; Liu, J.; Li, J. *J. Phys. Chem. Lett.* **2010**, *1*, 309.

JP912143P